

# Interaction dynamics of spatially separated cavitation bubbles in water

Nadine Tinne  
Silvia Schumacher\*  
Valeria Nuzzo\*  
Cord L. Arnold\*  
Holger Lubatschowski  
Tammo Ripken  
Laser Zentrum Hannover e.V.  
Hollerithallee 8  
30419 Hannover, Germany

**Abstract.** We present a high-speed photographic analysis of the interaction of cavitation bubbles generated in two spatially separated regions by femtosecond laser-induced optical breakdown in water. Depending on the relative energies of the femtosecond laser pulses and their spatial separation, different kinds of interactions, such as a flattening and deformation of the bubbles, asymmetric water flows, and jet formation were observed. The results presented have a strong impact on understanding and optimizing the cutting effect of modern femtosecond lasers with high repetition rates ( $>1$  MHz). © 2010 Society of Photo-Optical Instrumentation Engineers. [DOI: 10.1117/1.3526366]

Keywords: fs-laser; laser-induced optical breakdown; LIOB; laser-tissue interaction; photodisruption; cavitation bubble; ophthalmology.

Paper 10229PRR received Apr. 29, 2010; revised manuscript received Nov. 1, 2010; accepted for publication Nov. 1, 2010; published online Dec. 23, 2010.

## 1 Introduction

Three-dimensional processing inside transparent media by focused ultrashort laser pulses is utilized in various therapeutic applications of laser surgery in ophthalmology. Nowadays, there are well-established procedures, such as the LASIK procedure (*laser in situ keratomileusis*)<sup>1–5</sup> and keratoplasty, or future applications, such as femtosecond (fs)-Lentotomy<sup>6,7</sup> and laser cataract surgery.<sup>8</sup> Until recently, fs-laser systems with relatively high pulse energy ( $>1$   $\mu\text{J}$ ) and relatively low repetition rate (kilo Hertz regime) have been used in clinical applications.<sup>1</sup> A steady increase in the repetition rate of clinical laser systems,<sup>9,10</sup> along with lower applied pulse energies, has resulted in a significant reduction in treatment duration. Tight focusing with a large numerical aperture objective is frequently used,<sup>10</sup> offering better precision due to a smaller focal volume, a lower energy threshold for optical breakdown, and reduced collateral damage.

In the last few years, the interactions between the cavitation bubbles, generated by the laser-tissue interaction, have become very important in the context of medical laser applications. Whenever high repetition rate, ultrashort laser pulses are used to disrupt tissue in a liquid or biological environment, cavitation bubbles are produced, which interact with the tissue as well as with each other. The interaction between single laser pulses and biological tissue has been studied extensively, both experimentally and theoretically.<sup>11–16</sup> By focusing a laser pulse of fs duration to a small volume, very high intensities are easily accessible, initiating nonlinear absorption processes, such as multiphoton, tunnel, and cascade ionization, resulting in the generation of a dense free electron plasma.<sup>12,14,17,18</sup> The density of the generated free electrons and the plasma scales with the amount of energy deposited. If a critical electron density on

the order of  $\rho_{\text{cr}} = 10^{21} \text{ cm}^{-3}$  is exceeded, then an optical breakdown occurs.<sup>15</sup> Subsequently the following mechanisms appear: (i) the recombination of electrons with their parent ions heats the tissue, (ii) the pressure increases strongly localized, (iii) due to this buildup of mechanical energy a shock wave is created that propagates into the surrounding medium, and finally, (iv) a cavitation bubble forms.<sup>12,14,17,19</sup> The vapor-filled cavitation bubble undergoes a series of expansions and contractions, where the maximum radius depends on the fs-laser pulse energy.<sup>15</sup> For low pulse energies slightly exceeding the breakdown threshold, only one expansion and collapse of the bubble occur, causing the tissue to rupture; therefore, the effect of cutting tissue via a laser-induced optical breakdown (LIOB) is called photodisruption.

The interaction of cavitation bubbles generated by laser pulses that are spatially and temporally separated has scarcely been studied. Lauterborn<sup>20</sup> as well as Lauterborn and Hentschel<sup>21</sup> were the first to show, experimentally, that there is an interaction between adjacent cavitation bubbles generated by ns-laser pulses;<sup>20,21</sup> other groups were subsequently able to confirm these results experimentally.<sup>22–27</sup> Our interest in the detailed interaction dynamics of cavitation bubbles generated by fs-laser pulses was initially stimulated by previous work of ours, which showed that the cutting quality changes with increasing repetition rate and pulse energy.<sup>28</sup> An analysis of the generated laser dissection cuts suggests an interaction between the cavitation bubbles of two or more consecutive pulses in the course of the bubble's oscillation. Using low repetition rates in the range of some tens of kilohertz, a laser pulse only interacts with the final stage of effects generated by the previous pulse. In this case, subsequent pulses can be scattered from persistent gas bubbles or from tissue that is already ruptured. However, with greater repetition rates ( $>1$  MHz), it is possible that the cavitation bubble of the preceding pulse still exists when the next pulse approaches its proximity. The bubble oscillation time is on the order of microseconds duration;<sup>12,13,29</sup> thus, the next

\*Dr. Silvia Schumacher is currently at IROC AG, Switzerland. Dr. Valeria Nuzzo is currently at Harvard University, Cambridge, MA. Dr. Cord L. Arnold is currently at Lund University, Sweden.

Address all correspondence to: Nadine Tinne, Laser Zentrum Hannover e.V., Hollerithallee 8, 30419 Hannover, Germany; Tel: 49-511-2788-212; Fax: 49-511-2788-100; E-mail: n.tinne@lzh.de

created bubble starts to expand and collapse while the previous is still present. The interaction between cavitation bubbles may cause collateral damage to sensitive tissue structures in the vicinity of the laser focus, and it may also contribute in several ways to ablation and cutting dynamics: (i) by disruption caused during bubble expansion, (ii) by jet formation pointing toward still unaffected tissue, or (iii) by tensile stress exerted during bubble collapse. The focus of the experiments presented here is the characterization and understanding of the fundamental interaction of subsequently generated cavitation bubbles. This is of great interest for the prospective optimization of the surgical process with high repetition rate femtosecond lasers.

The present study describes systematic experimental investigations of the dynamics of two spatially separated laser-induced cavitation bubbles. The cavitation bubble dynamics and the interaction mechanisms were examined by time-resolved photography. The overall motion of the bubbles was investigated by changing the time delay between the laser pulse and the illumination by a nanosecond flash lamp. A parallel exposure of the focus region according to Koehler illumination provided the optimal contrast for the boundary deformation and liquid jet penetration into the surface of the cavitation bubbles. In the present study, two parameters were varied: first, the distance of the cavitation bubbles, and second, the energy ratio of the laser pulses generating the bubbles. The bubble-bubble interaction features a vast complexity with sensitive dependence on the investigated parameters.

The experiments presented here reflect not strictly the conditions found in a surgical laser-scanning process, where pulses are applied with the same pulse energy but subsequently. Therefore, the results of our study are discussed with respect to collateral damage in laser surgery and cavitation bubble-mediated enhancement of tissue cutting.

## 2 Materials and Methods

The experimental setup allows for the generation of two cavitation bubbles by focused laser pulses and the imaging of their dynamics by time-resolved photography.

### 2.1 Generation of Spatially Separated Cavitation Bubbles

A schematic diagram depicting the experimental arrangement used to investigate the interaction of two spatially separated cavitation bubbles is shown in Fig. 1. The bubbles were generated in a cuvette made of PMMA (polymethyl methacrylate) and filled with distilled water.

The fs-laser (Bright, *Thales*, Orsay, France) emits pulses of  $\tau = 125$  fs duration at a wavelength of  $\lambda = 780$  nm at a repetition rate of 5 kHz. For our application, the repetition rate is reduced to 20 Hz. The beam is split between two arms using a polarizing beamsplitter; the relative energy of the two pulses can be adjusted with a half-wave plate.

The two beams are overlaid again and copropagate through a telescope ( $f_1 = 100$  mm,  $f_2 = 300$  mm), which is used to expand the beam and to overfill the back aperture of the focusing objective. In order to avoid interfaces and to provide good focal quality, a water immersion objective (HCX APO L 20x/0.50 W U-V-I/D 3.5, *Leica*, Wetzlar, Germany) with numerical aperture NA = 0.5 is used. Because of the good transparency and high water content of biological tissue<sup>21,30</sup> and its similar optical, mechanical, as well as thermodynamic properties, water is used as a model substance for the transparent tissue of the crystalline lens or the cornea.

The spatial separation of both laser foci is realized by a pivotable mirror, introducing a small angle between the two beams when entering the focusing objective. Hence, the regions of optical breakdown are spatially separated in the focal plane, but both breakdowns occur at the same time.

### 2.2 Time-Resolved Photography

Time-resolved photography permits the analysis of fast dynamic phenomena by sectioning the process in specific events. The observation of the oscillating cavitation bubbles is realized by stroboscopic illumination with a nanosecond flash lamp (KL-M, *High-Speed Photo Systeme*, Wedel, Germany) with 12-ns spark duration. The illumination path is arranged perpendicular to the direction of laser focusing (Fig. 2). Under Koehler

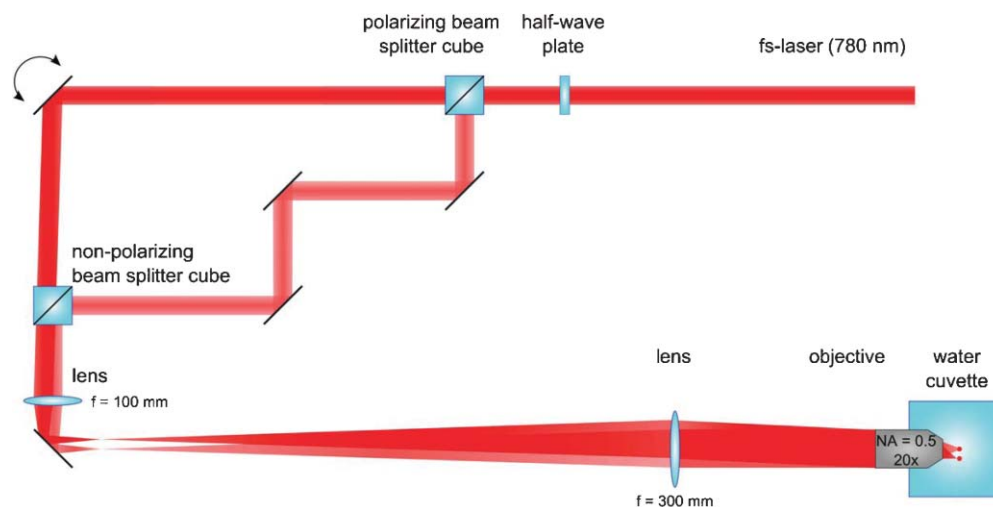


**Fig. 1** Experimental setup of the laser system (top view). The fs-laser beam is split into two laser arms with a variable angular offset to create spatially separated regions of laser-induced optical breakdown and, hence, cavitation bubbles inside the water cuvette.

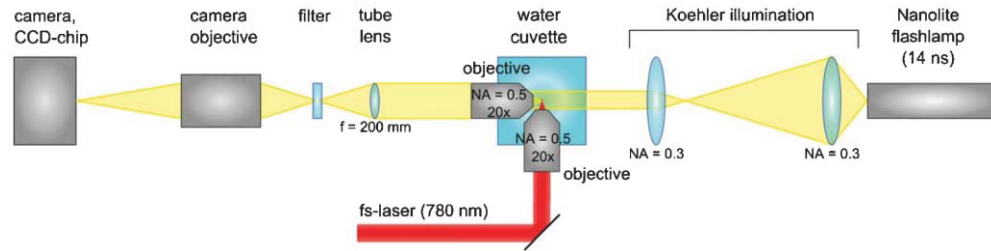


**Fig. 2** Illumination path for time-resolved photography (side view). Because of the Koehler illumination the water cuvette is illuminated homogeneously by the spark of the flash lamp. A microscope objective, in combination with a tube lens and a camera objective, generates a magnified, sharp image of the cavitation bubbles on the CCD chip of the camera.

illumination,<sup>21</sup> which is also used for bright-field microscopes, the plane of the optical breakdown is illuminated homogeneously. The observation path consists of a second  $NA = 0.5$  water immersion microscope objective (HCX APO L 20x/0.50 W U-V-1/D 3.5, *Leica*, Wetzlar, Germany), arranged confocally with the focusing objective, an adjusted tube lens, and a camera zoom objective. This configuration provides a magnified and sharp image (dimensions approx.  $176 \times 265 \mu\text{m}$ , magnification 90x) on the CCD chip of the camera (D70, *Nikon*, Tokyo, Japan).

The controlling and timing is realized by a delay generator (DG102, *Bergmann Messgeräte Entwicklung KG*, Murnau, Germany). By changing the delay of the flash lamp spark in respect to the laser pulse, images at different stages during the bubble oscillation are recorded. The dynamics of expanding and collapsing cavitation bubbles can be reconstructed and illustrated by lining up single frames of different bubbles at subsequent delays.

### 2.3 Experimental Procedure

In this study, we performed two kinds of experiments. First, we analyzed the interaction of two cavitation bubbles with the same energy by varying only the bubble separation; afterward, we varied both the relative pulse energies and the bubble separation. Although the first approach does not strictly reflect a surgical laser-scanning process (see also Section 1), it facilitates a comparison to earlier experimental results (cf. the analogy to cavitation bubble dynamics near solid boundaries described in Section 4) and to allow an analysis of the fundamental characteristics of the interaction of two cavitation bubbles. The latter sce-

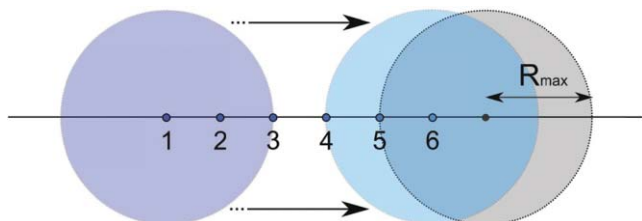


**Fig. 3** Schematic diagram of the six measurement positions used to observe the interaction dynamics of two cavitation bubbles of the same laser pulse energy. While the right bubble is fixed as a reference, the position of the left bubble is varied in six steps, ranging from 3.0 times  $R_{\text{max}}$  to 0.5 times  $R_{\text{max}}$  (center to center).

nario, however, replicates the physical separation, energy, and difference in oscillation phase of cavitation bubbles produced by laser scanning during medical treatment. In our experiments, this difference in oscillation phase is based on the different laser pulse energies creating the cavitation bubbles. In the event of a laser surgery, it is caused by the scanning process and, hence, a temporal separation of equally sized cavitation bubbles. In both cases, the intensity and mode of interaction varies with the distance between the bubbles.

We studied the dynamic interaction of two cavitation bubbles of the same energy at a variable distance. The distance is scaled in units of the maximum bubble radius  $R_{\text{max}}$ . We compare six bubble separations between  $3.0 \times R_{\text{max}}$  and  $0.5 \times R_{\text{max}}$  (center to center), as sketched in Fig. 3.

Similar to our study of the interaction of equally sized cavitation bubbles (see Section 3.1), we also analyzed the interaction of two bubbles created with different pulse energies. In this case, the distance from the surface of the larger cavitation bubble to the center of the smaller one is scaled in units of the maximum bubble radius of the smaller bubble, which we will refer to as  $r_{\text{max}}$  in order to differentiate it from the case of the equally sized bubbles. The separation is varied in nine steps, from  $-1.0 \times r_{\text{max}}$  to  $3.0 \times r_{\text{max}}$ ; this is illustrated in Fig. 4. The smallest separation corresponds to a complete overlap of the expanded bubbles.

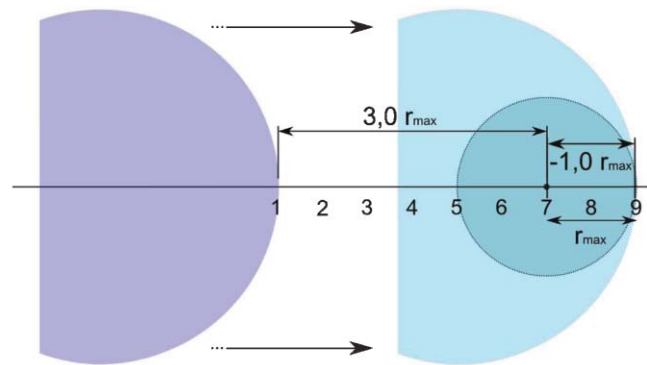


**Fig. 4** Schematic diagram of the nine measurement positions used to observe the interaction dynamics of two cavitation bubbles generated at different laser pulse energy. While the smaller bubble on the right is fixed as a reference, the position of the left bubble, which is generated with higher laser pulse energy, is varied in nine steps, ranging from 3.0 times  $r_{\text{max}}$  to  $-1.0$  times  $r_{\text{max}}$  (surface to center).

### 3 Results

#### 3.1 Dynamics and Interaction of Two Bubbles with the Same Energy

Figure 5 illustrates the interaction dynamics of two cavitation bubbles, which are generated at a distance of 3.0 times  $R_{\max}$  (center to center) at different time stages. The bubbles were each created at a pulse energy of 2.0 times the breakdown threshold each (which corresponds to 120 nJ) and hence are of nearly the same size. The images were taken with a time delay step of 0.1  $\mu\text{s}$ , where the jitter of the flash lamp adds an uncertainty of  $\sim 50$  ns. However, for the sake of simplicity, images are labeled and referred to by the delay only.

After application of the laser pulses, two cavitation bubbles form as a result of LIOB. Because the Rayleigh range is much larger than the transverse focal spot size, the bubbles initially grow in a prolate shape along the direction of laser propagation (see Fig. 5, at 0.3  $\mu\text{s}$ ). From 0.3 to 1.5  $\mu\text{s}$ , the bubbles expand undisturbed from each other and feature almost spherical shape. They reach their maximum radius of  $\sim 16$   $\mu\text{m}$  (which coincides with the size of a single bubble obtained with the same energy) at 1.9  $\mu\text{s}$ . As the two expanded bubbles approach each other, the inner boundaries tend to flatten slightly (see images taken at 1.9 and 2.1  $\mu\text{s}$ ). Afterward the bubbles start to collapse asymmetrically, and to become elongated along their connecting line; this can be observed at 3.3  $\mu\text{s}$ . The collapse phase ends as funnel-shaped indentations develop at the outer boundaries of both bubbles at 3.7  $\mu\text{s}$ , followed by the formation of two opposing water jets (not seen in the images, because bright-field photography is only sensitive to refractive index changes). After the complete collapse of both bubbles, a single cavitation bubble forms at 4.1  $\mu\text{s}$ , a second expansion of only one cavitation bubble with an oblate shape at the center of mass is observable (compare images in Fig. 5 at 4.2 and 5.0  $\mu\text{s}$ ). The second maximum in bubble size is reached at 5.0  $\mu\text{s}$ . After this second oscillation, the new bubble finally collapses (see, for example

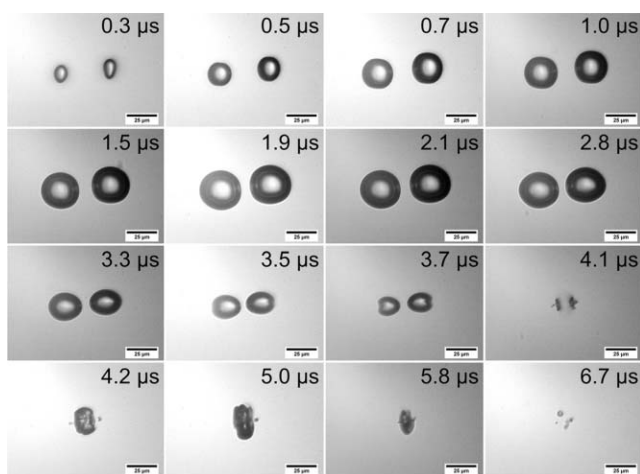


**Fig. 5** Dynamics of the interaction of two spatially separated cavitation bubbles generated with a laser energy of 120 nJ (corresponding to 2.0 times the breakdown threshold) and a distance of 3.0 times  $R_{\max}$  (center to center). Only the images at the most relevant delays are shown in order to illustrate the interaction mechanisms. The laser propagation direction is top down in these images due to the optical path in the illumination path.

Fig. 5 at 5.8  $\mu\text{s}$ ) and a cloud of persistent gas bubbles remains in the focal volume (see 6.7  $\mu\text{s}$ ).

Figure 6(a) shows the bubble radii and Fig. 6(b) shows the distance of the centers of mass as a function of time. Although the radii presented are from one measurement, the distance of the centers of mass is an average of five measurements. The measurement error of  $\pm 2$   $\mu\text{m}$  is mostly due to the temporal jitter of the illumination. The maximum radii and the oscillation durations of the cavitation bubbles created in pairs show similar characteristics as for a single bubble. Both bubbles reach their maximum radius of  $\sim 16$   $\mu\text{m}$  at 1.9  $\mu\text{s}$  and collapse completely at 4.1  $\mu\text{s}$ . The second oscillation cycle shown in Fig. 6(a) corresponds to the secondary bubble formed at their common center of mass. Here, the oblate deformation becomes apparent by exhibiting that the maximum radius in the axial direction, at 13.6  $\mu\text{m}$ , is clearly larger than in the radial direction, where the radius is 8.5  $\mu\text{m}$ . At 6.6  $\mu\text{s}$  the oscillation cycle of the secondary bubble is complete, and we believe that further analysis of the radii during the gas bubble phase is not instructive. The distance of the centers of the two cavitation bubbles was determined until their collapse at 4.1  $\mu\text{s}$  [see Fig. 6(b)]. Whereas during the expansion phase the separation is almost constant at  $\sim 42$   $\mu\text{m}$ , it reduces to 12  $\mu\text{m}$  during the collapse phase.

The type and intensity of the different interaction mechanisms, such as, for example, a second oscillation cycle of both cavitation bubbles or one new bubble at the common center of mass as well as the fusion of the bubbles, change with the distance between the two cavitation bubbles. Figure 7 shows a qualitative evaluation of all series of measurements. Laser pulse energy is plotted against bubble distance; each measurement point is indicated by a black spot in the diagram. Additionally, the shaded areas refer to different interaction mechanisms. In most cases [more than four positions of measurements at three different pulse energies of 1.5 times (90 nJ), 2.0 times (120 nJ), and 3.0 times breakdown threshold (180 nJ)], a second oscillation cycle of a newly formed bubble at the center of mass of both bubbles is observed. Only for two analyzed cases, at laser pulse energies of 1.5 times and 3.0 times breakdown threshold and a bubble separation of  $3.0 \times R_{\max}$ , a second oscillation cycle of both individual bubbles was observed. For 180 nJ and a separation of  $3.0 \times R_{\max}$ , the bubbles reappear in close proximity after the first collapse but can still be identified separately during the second oscillation cycle.

For separations of  $< 2.0 \times R_{\max}$ , the surfaces of the cavitation bubbles touch each other as expected from geometrical considerations (cf. right side of the vertical dashed-dotted line in Fig. 7). Fusion of the bubbles occurs only at a very small bubble distance of  $< 0.5 \times R_{\max}$ . In this case, the cavitation bubbles appear and expand to their maximum volume, still separately identifiable, but merge together at the beginning of the collapse phase until it is not possible to differentiate the two bubbles. For bubble separations between these two extreme values, the flattening, the jet intensity, and the amplitude of the reexpansion depend on the initial spatial separation of the bubbles.

#### 3.2 Dynamics and Interaction of Two Bubbles with Different Energies

Two bubbles generated with different laser pulse energies feature different interaction mechanisms from the ones described

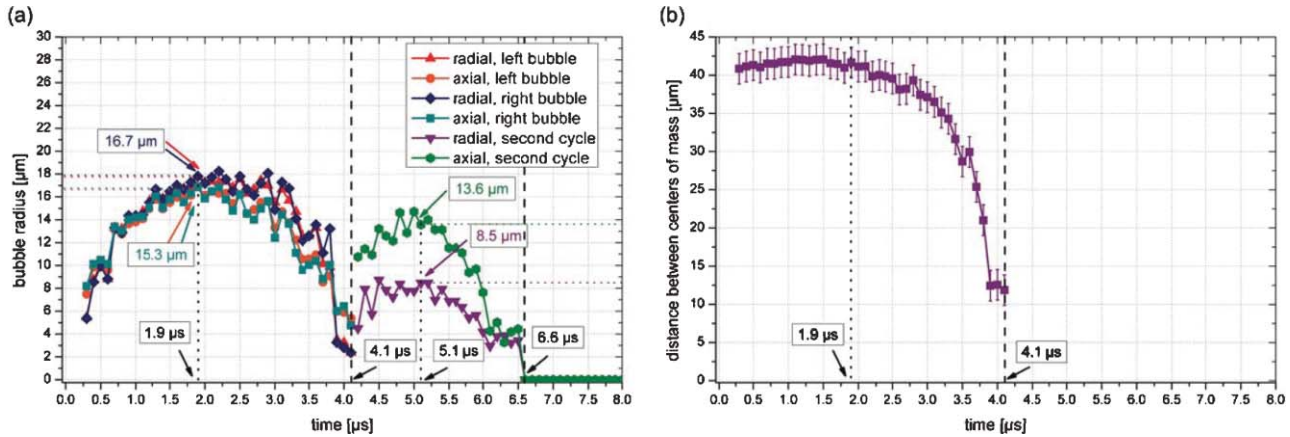


**Fig. 6** Analysis of the interaction dynamics of two spatially separated cavitation bubbles generated at 2.0 times the breakdown threshold at a distance of 3.0 times  $R_{max}$ . (a) The bubble radii for both cavitation bubbles as well as their second oscillation cycles are plotted in radial and axial direction, respectively, against time. (b) The distance between the centers of mass is plotted against time until the complete bubble collapse of the first oscillation cycle.

in Section 3.1. Again, the interactions strongly scale with the distance between the bubbles. Figure 8 shows the dynamics of two representative cavitation bubbles obtained with energies of 150 nJ (left) and 120 nJ (right), corresponding to 2.5 times and 2.0 times the breakdown threshold respectively, at a distance of  $3.0 \times r_{max}$ .

Initially, the two bubbles expand undisturbed by each other. The shape again is prolate in the direction of laser propagation (see Fig. 8, at 0.3 μs). Because the bubble separation is large, the interaction during the expansion phase is negligible. The bubble shape is spherical until  $\sim 1.2 \mu s$ , after which it becomes oblate in the laser propagation direction.

The bubble generated with the lower energy achieves its maximum radius of  $\sim 16.0 \mu m$  at 1.9 μs, and starts to collapse first. This leads to the formation of a prolate bulge of the right side of

the larger bubble, which continues to expand to reach its maximum radius of  $\sim 22.0 \mu m$  at 2.3 μs. When the smaller bubble collapses, a funnel-shaped indentation develops (for example, see Fig. 8 at 3.2 μs) and a water jet forms, directed toward the other cavitation bubble. The water jet can be observed as a horizontal shadow inside the right bubble (see 3.5–4.3 μs). Both bubbles start to expand again in the vertical direction after their complete collapses at 3.5 and 4.3 μs, respectively. Following their second collapses, two gas bubbles remain at the focus region (see Fig. 8 at 5.5 μs).

Bringing the two bubbles closer with a center-to-center distance of  $1.5 \times r_{max}$ , leads to a total change in the interaction dynamics, as depicted in Fig. 9. When the smaller cavitation bubble (right side) reaches its maximum radius and enters the collapse phase, a funnel-shaped indentation forms between 3.2 and 3.5 μs, and a water jet forms during the collapse phase

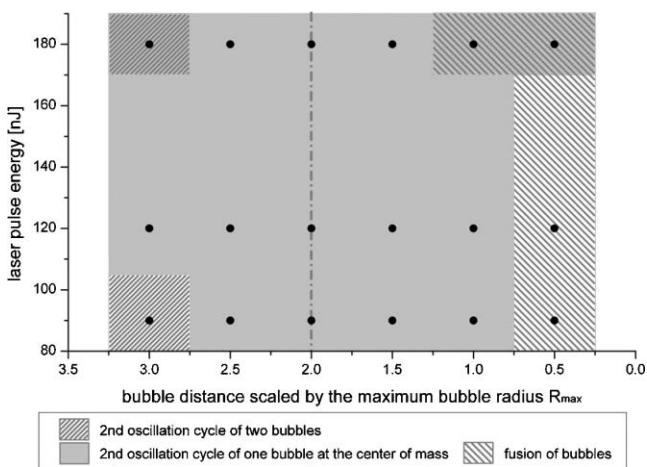


**Fig. 7** Schematic diagram of qualitative comparison of the different interaction mechanisms, depending on the laser pulse energy as well as the bubble separation scaled in  $R_{max}$ . The black dots mark the points of measurement. The shaded areas illustrate the different regimes of interaction dynamics observed. For bubble distances smaller than the dashed-dotted line contact between the bubble surfaces can be observed. More than one effect may occur at an individual point of measurement, which is labeled by a combination of the particular shades and frames.

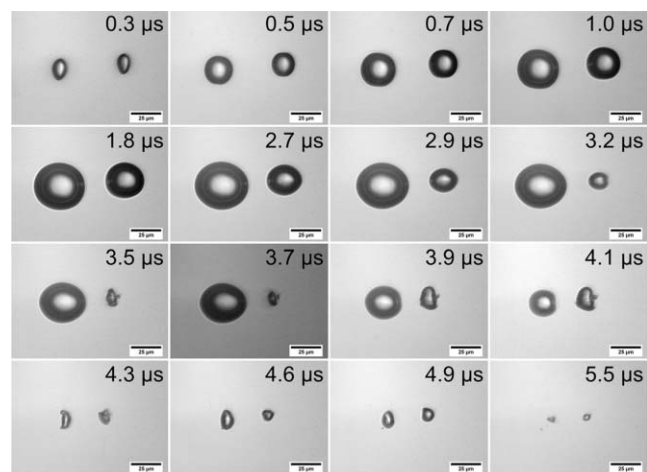


**Fig. 8** Dynamics of the interaction of two spatially separated cavitation bubbles generated at laser pulse energies of 2.5 times (left bubble) and 2.0 times (right bubble) the breakdown threshold corresponding to 150 and 120 nJ, respectively, and at a distance of 3.0 times  $r_{max}$ . Only the images at the most relevant delays are shown in order to illustrate the interaction mechanisms. Again, the laser propagation direction is top down in these images due to the optical path in the illumination path.

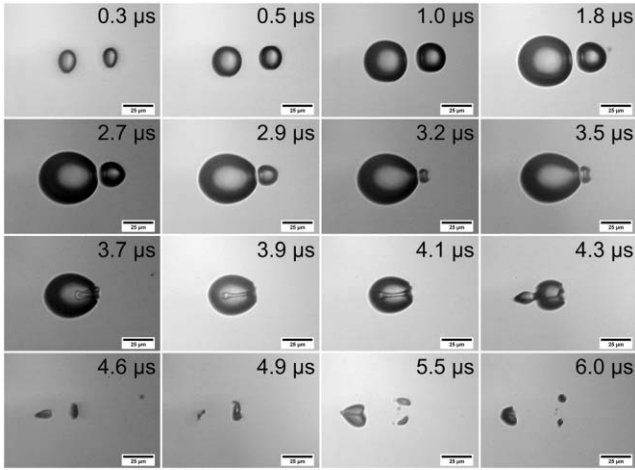


**Fig. 9** Dynamics of the interaction of two spatially separated cavitation bubbles generated at the same pulse energies as in Fig. 8 at a distance of 1.5 times  $r_{max}$ . The laser propagation direction is top down in these images due to the optical path in the illumination path.

(see 3.5  $\mu s$ ). Because of the bubbles' proximity, the water jet is able to reach the left cavitation bubble, traverse it, and re-emerge from the opposite surface at 4.3  $\mu s$ . There, a new cavitation volume forms, which also features a characteristic oscillation (see

images in Fig. 9 from 4.6 to 6.0  $\mu s$ ). A gas bubble remains after its collapse. Because of the considerable oblate deformation and the cone-shaped water flow, the larger bubble splits into two gas bubbles (see images 5.5 and 6.0  $\mu s$  in Fig. 9) (cf. Ref. 31).

Figures 10(a) and 10(c) shows the bubble radii and Figs. 10(b) and 10(d) show distances between the centers of mass as functions of time, obtained for the experimental conditions corresponding to Figs. 8 and 9, respectively. As before, the analysis of the distance between the centers of mass was averaged over five measurements with a resulting deviation of  $\pm 2 \mu m$ , which can in turn be explained by the jitter of the illumination. In both cases, the left bubble is much larger than the right one and reaches its maximum radius up to 1  $\mu s$  later. In Fig. 10(a), the second oscillation cycle of each cavitation bubble starts even before a complete collapse appears. In contrast, Fig. 10(c) shows the jet formation after the collapse of the smaller right bubble as an intense increase of the radius in the radial direction.

The distances between the centers of mass initially increase slightly ( $\sim 8 \mu m$ ) for both cases studied. However, when the smaller bubbles reaches their maximum expansion after 3.5 and 3.6  $\mu s$ , respectively, the left and right bubbles start to approach each other [see Figs. 10(b) and 10(d)]. The center-of-mass distance continues to decrease after the first collapse of the left bubble. In the case of comparatively closer bubbles, the

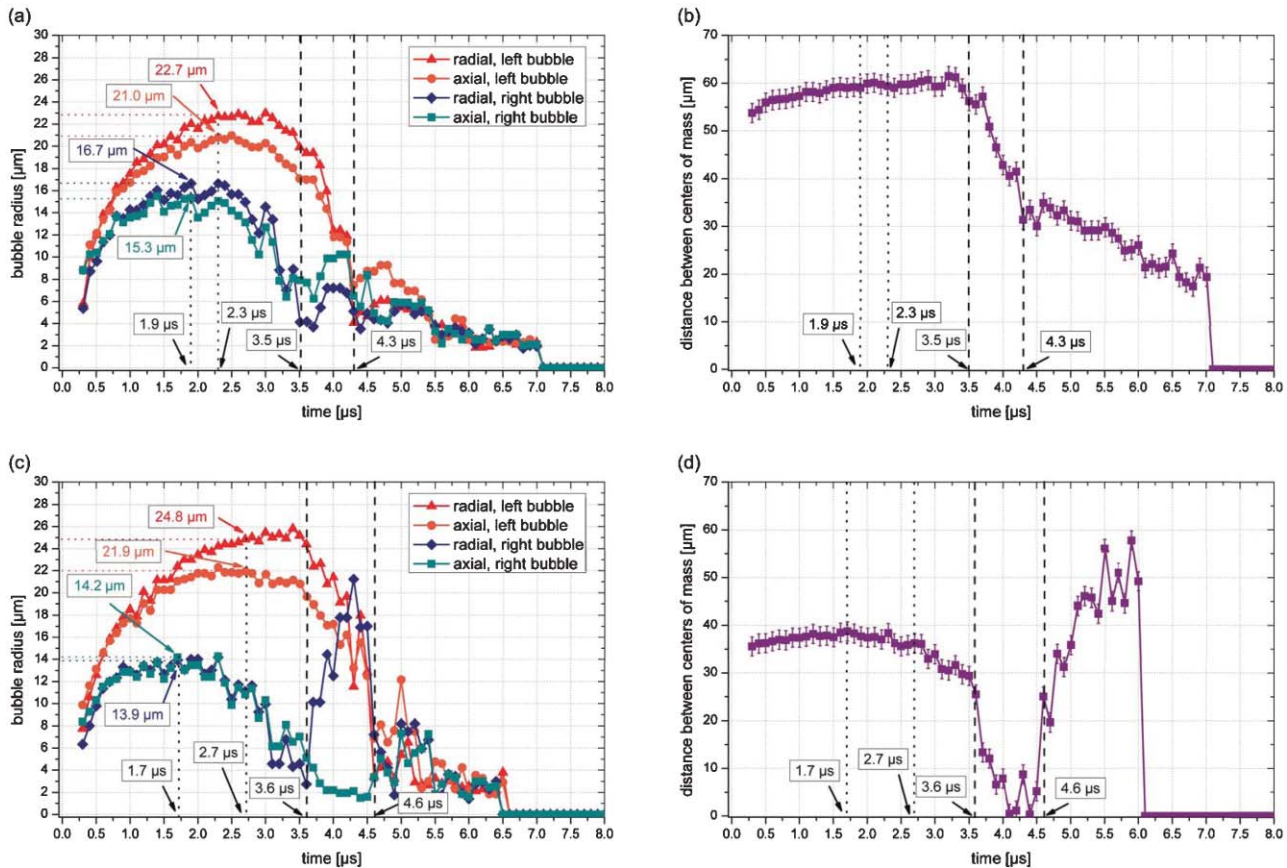


**Fig. 10** Analysis of the series of measurements of the interaction dynamics of two spatially separated cavitation bubbles generated with an energy ratio of 2.5:2.0 (in units of the breakdown threshold) and a distance of 3.0 times and 1.5 times  $r_{max}$ , respectively. (a,c) The bubble radii of both cavitation bubbles are plotted for both the radial and axial directions as functions of time until the complete bubble collapse of the first oscillation cycle. The vertical lines mark the times of the maximum bubble radius (dotted) as well as the first bubble collapse (dashed).

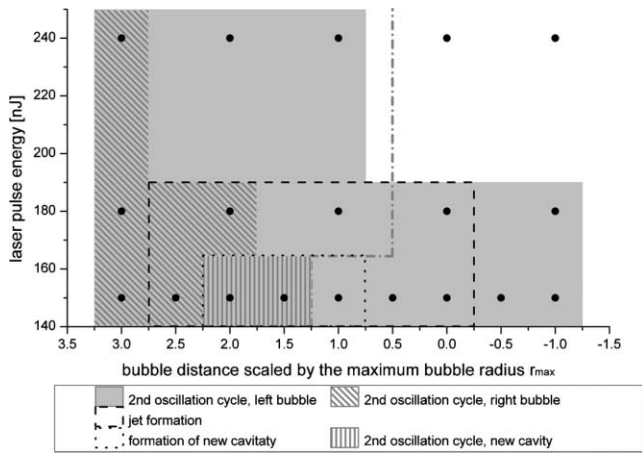


**Fig. 11** Schematic diagram of qualitative comparison of the different interaction mechanisms depending on the laser pulse energy of the comparatively larger cavitation bubble [the other bubble was created with 2.0 times breakdown threshold (120 nJ) in each case] as well as the bubble distance scaled in units of  $r_{max}$ . The black dots mark the points of measurement; the shaded or framed areas are interpolated based on the results. For bubble distances smaller than the dashed-dotted line contact between the bubble surfaces can be observed. Additionally, a second oscillation cycle of each bubble, jet formation (inside dashed line), the formation of a new cavitation volume (inside dotted line), and a second oscillation cycle of this cavity could be detected. More than one effect may occur at an individual point of measurement, which is labeled by a combination of the particular shades and frames.

center-of-mass distance rebounds after  $4.6 \mu\text{s}$  with the formation of a new cavitation bubble [Fig. 10(d)].

The mechanisms of interaction differ strongly, depending on the distance of the bubbles as well as the energy ratio of the laser pulses. The schematic diagram in Fig. 11 shows the qualitative evaluation of all series of measurements. The laser pulse energy corresponding to the more energetic cavitation bubble is plotted against the bubble distance. The black dots mark the performed measurements. Additionally, differently shaded and sectioned areas refer to different interaction mechanisms. A second oscillation cycle of the larger bubble can be observed in almost all cases. Contrary, the right bubble shows a second oscillation cycle only for distances of  $>2.0 \times r_{max}$ , owing to a weaker interaction.

For the two smaller energy ratios studied [(2.5:2.0) times and (3.0:2.0) times the breakdown threshold], the two bubbles draw closer together during the expansion and collapse phases, causing increased interaction. This leads to the formation of a water jet due to an asymmetric collapse of the smaller bubble, which traverses the left bubble. For the smallest energy ratio of (2.5:2.0) times the breakdown threshold and bubble distances of 1.0 times to 2.0 times  $r_{max}$ , this water jet gives rise to a new phenomenon: after traversing the larger bubble, the water jet penetrates the far side and creates a new cavitation volume with its own oscillation cycle. Again, the bubble surfaces touch during the expansion phase for distances of  $>2.0 \times r_{max}$ . Contrary to geometrical expectations, no contact between the bubbles is observed for energy ratios of (4.0:2.0) times and (3.0:2.0) times breakdown threshold at a distance of  $1.0 \times r_{max}$ .

## 4 Discussion

As the repetition rate of modern clinical ultrashort laser pulse systems continuously increases, the understanding of the interaction of cavitation bubbles generated close to each other in space and time has become very important in order to optimize the cutting process. The purpose of our study is to investigate the interaction of two spatially separated cavitation bubbles and to characterize the different interaction mechanisms. Years ago, Lauterborn<sup>20</sup> as well as Lauterborn and Hentschel<sup>21</sup> reported the occurrence of oscillation dynamics which demonstrate the interaction of two spatially separated cavitation bubbles obtained at constant laser energy and bubble distance. Even though the pulse durations were in the nanosecond regime, resulting in large cavitation bubbles of millimeter size, the results are in agreement with our current findings. The interaction of two spatially separated cavitation bubbles was also addressed experimentally and numerically by other researchers. Mostly two bubbles were analyzed near a rigid boundary in order to study the mechanical consequences of multibubble interaction close to solid surfaces, but their preliminary experiments also investigated the case of bubble–bubble interaction without a boundary closeby.<sup>22–27,32,33</sup> The observations reported in these studies are also in agreement with the results described here and will be discussed in detail later.

As presented in Section 3, the complex bubble-bubble interaction depends both on the energy ratio and the initial bubble separation.<sup>25,33–35</sup> Initially, we studied the dynamics and interactions of two bubbles generated by pulses of the same energy (Section 3.1). In this case, the bubbles have almost the same size; each behaving like a single bubble near a plane rigid boundary,<sup>36–42</sup> which is placed at half the bubble separation.<sup>22–26,32,33,43</sup>

According to Vogel *et al.*,<sup>30</sup> the initial bubble shape follows the focal volume at the onset of the expansion, featuring an elongated initial bubble along the Rayleigh length, which is much larger than the transverse beam size at low-to-medium NA focusing, as used in this study. Afterwards, the bubble shape changes to a spherical, as observed before by Akhatov *et al.*,<sup>44</sup> Geisler,<sup>45</sup> and Tomita *et al.*<sup>44–46</sup> as well as Heisterkamp,<sup>47</sup> who suggests the influence of the surface tension for the change of shape. During the subsequent collapse phase, the conservation of momentum in consideration of the moving bubble surface leads again to an oblate deformation, but this time perpendicular to the direction of laser propagation.<sup>47</sup>

During the expansion phase, only a weak interaction between the two bubbles is observed. As the bubble surfaces approach each other during the expansion phase, the cavitation bubbles become flattened, which is attributed to a compression of the water volume between the two bubbles.<sup>23,25–27,33,34,48</sup> It is conceivable that due to the comparably slow propagation of the water, only a part of the water volume flows outwardly,<sup>26</sup> but predominantly an intense increase of pressure develops in the water channel encased between the expanding bubbles. This volume of high-pressure incompressible water prevents the further approach of the bubble surfaces, initiating a flattening of the bubble surfaces instead.<sup>23,27,48</sup>

Following the expansion phase, the individual bubbles collapse asymmetrically because the flow of incoming water is hindered by the other bubble. The similarity to the case of a

cavitation bubble near a rigid boundary is obvious.<sup>32,36,39,41</sup> The flow of water along the axis connecting the two bubbles is less than in the perpendicular direction. As a consequence, the collapse along that direction occurs faster, which induces a prolate, bulged deformation of the collapsing bubble. Additionally, in the direction given by the line connecting the two bubbles, the outward water flow from the volume between the bubbles is less than the flow incoming from the outermost bubble surfaces. Thus, two counterpropagating water jets form, penetrating each bubble directed toward their common center of mass.<sup>22–25,27,32,34</sup> Like Quinto-Su and Ohl,<sup>23</sup> we observed an attraction between the bubbles that accompany the jet formation described above, and that is related on the bubble distance according to the absolute value of bubble movement.<sup>22–25,27,33,34</sup> The bubble shape during the bubble-bubble interaction as well as the movement of each bubble's center of mass toward the "boundary" described above shows a very close resemblance to a cavitation bubble that is collapsing near a rigid boundary.<sup>36–38</sup>

Ohl and Ory, who analyzed the asymmetric bubble collapse of one bubble near a rigid boundary, observed a faster decrease of the bubble volume if the water jet impacts the opposite bubble wall.<sup>35</sup> Contrary, Blake and Gibson<sup>36</sup> as well as Testud-Giovanneschi *et al.*<sup>36</sup> observed longer of the bubble lifetime near a rigid boundary. We could not verify this effect for the comparable case of two spatially separated and equally sized cavitation bubbles. Our experiments showed a correlation between the oscillation period of the two-bubble system and the single-bubble oscillation in the range of  $\pm 100$  ns.

The two water jets collide at the center of mass of both bubbles and increase the pressure of the water volume even more. This corresponds to a water jet of a single-cavitation bubble directed toward a rigid boundary.<sup>36</sup> Originating from the resulting, strongly localized high-pressure region, which is comparable to the situation after the laser-induced optical breakdown, a secondary shock wave is expected to propagate into the surrounding water<sup>36–42</sup> (cannot be proven by the technique of shadow photography). As a result of these collapse mechanisms, another cavitation bubble forms at the center of mass. The water jet continues to flow inward, as evidenced by shadows inside the bubble, resulting in an oblate profile. The second collapse results in a cloud of remaining gas bubbles, which is consistent with persistent inward water flow. Likewise, the convergence of the collapsing bubbles shown in Fig. 6(b) suggests the presence of water jets. The experiments of Lauterborn and Ohl<sup>22</sup> show a second oscillation cycle as well. To our best knowledge, an oscillation of a single-cavitation bubble at the common center of mass has not been reported before.

In the case of two equally sized cavitation bubbles, we observe a second oscillation cycle for each bubble only for comparably large distances and, hence, a weak bubble-bubble interaction (cf. Section 3.1); this case is investigated by Lauterborn and Ohl.<sup>22</sup> By contrast, only for very small bubble distance and, therefore, a large bubble overlap do the two bubbles merge during collapse. This mechanism may be caused by the close proximity and, hence, the flattening of the bubbles during expansion. This arrangement minimizes the water volume between the bubbles, which results in a nearly spherical inward flow with the beginning of the collapse phase. Whereas Quinto-Su and Ohl<sup>23</sup> did not observe bubble coalescence for their chosen initial separation due to a strong interaction, Testud-Giovanneschi *et al.*<sup>33</sup>

saw a bubble coalescence occurring only after the simultaneous implosion of two similarly sized bubbles; the simulations of Rungsiyaphornrat *et al.*<sup>27</sup> afford a criterion for the thickness of the water film between the two cavitation bubbles, which accompanies bubble fusion.

In comparison, the dynamics and interaction of two cavitation bubbles with different energies are similar at the initial phase of the bubble generation, but the later the dynamics differ from bubbles generated at the same energy. Again both cavitation bubbles appear prolate in shape and become more spherical during the process of expansion. The water pressure between the bubbles increases as the bubble surfaces converge, and a deformation in the form of a flattening is observed, analogous to the case of two bubbles created with the same laser pulse energy.<sup>23,25–27,33,34,48</sup>

Different oscillation durations are characteristic of bubbles generated at unequal laser energies, although bubble-bubble interaction depends strongly on the energy ratio and the bubble distance is reported in this case as well.<sup>24–26,33,34</sup> Generally, the duration of one oscillation cycle of a cavitation bubble depends on the laser pulse energy. Thus smaller bubbles generated at lower energy feature a faster oscillation and a smaller maximum radius.<sup>18,20,21,30</sup> Therefore, the smaller bubble reaches its maximum radius and starts to collapse while the more energetic one is still expanding. During the collapse of the smaller bubble, there is asymmetric inward water flow, because water flows from the region between the bubbles. At first, a funnel-shaped indentation is induced in the smaller bubble (*e.g.*, in Fig. 8 at  $3.2 \mu\text{s}$ ). After the complete collapse of the smaller bubble, this indentation results in a water jet directed toward the larger, existing bubble.<sup>25</sup> The jet formation is accompanied by convergence of the bubbles in the final collapse stage, as observed by Quinto-Su and Ohl<sup>23</sup> among others.<sup>25,34</sup> Shima<sup>24</sup> and Tomita *et al.*<sup>25</sup> report repulsion of the smaller bubble from the larger one, which we verify for the expansion phase of the smaller bubble in our experiments. In contrast, neither group investigated a bubble distance that leads to a jet formation. During the collapse of the smaller bubble, the larger cavitation bubble also reaches its maximum radius and begins to collapse. The inward water flow toward the collapsing larger bubble, which is inhibited in the direction of the smaller bubble, and the influx of water towards the collapsing smaller bubble, promotes the formation of a prolate bulge at the surface of the higher energetic bubble.<sup>23</sup>

Despite the influence of the smaller bubble, the larger bubble undergoes a second oscillation cycle in nearly all observed cases (cf. Section 3.2). Tomita *et al.*<sup>25</sup> and Testud-Giovanneschi *et al.*<sup>33</sup> also report that the influence of a small bubble on another larger bubble is comparatively weak. The water jet, which can be observed inside the cavity during this second oscillation cycle of the cavitation bubble, is a sign of continued water flow. Additionally, analysis of the center of mass distance shows an increased distance between the higher energetic cavitation bubble during its second oscillation cycle and the left-sided novel cavity [see bubble after  $4.6 \mu\text{s}$  in Fig. 10(d)], which supports the idea of long-lasting water flow proposed before.

For one cavitation bubble near a solid boundary,<sup>36</sup> as well as for two interacting cavitation bubbles,<sup>25,26</sup> we expect an increase in the smaller bubble's motion period of oscillation. We observe an increase of  $\sim 250$  ns, in qualitative agreement with explanations.

The asymmetry of water flow leading to the collapse of the smaller bubble is governed by the bubble distance as described in Section 3.2; hence the magnitude of the water hammer pressure is a function of bubble distance.<sup>35</sup> Similarly, Shima<sup>24</sup> and Tomita *et al.*<sup>26</sup> showed that the smaller bubble is significantly influenced by the pressure field resulting from the motion of the neighboring larger bubble. For comparably large bubble distances, the influence of the larger bubble on the collapse of the smaller bubble is relatively weak; even the smaller bubble undergoes another oscillation cycle after the first collapse. At shorter bubble distances, the water jet formed from the smaller bubble reaches the larger bubble still in its oscillation phase. After a short period, it can traverse the bubble and break through its backside due to the inertia of the water.<sup>25</sup> For the series of measurements with an energy ratio of (2.5:2.0) times the breakdown threshold, the water jet is intense enough to produce a new cavitation volume at the backside of the water-penetrated cavity. Possibly, the impact of the highly accelerated water jet on the water volume at the back wall of the cavitation bubble compresses the medium so strongly that a shock wave occurs and a new cavitation bubble forms. The assumption that the observed shadow corresponds to a cavitation bubble is supported by the observation of oscillations in two analyzed cases. Lauterborn and Ohi<sup>22</sup> describe similar bubble development of one cavitation bubble near a rigid boundary. There, a so-called ‘tip bubble’ is created between the jet “tip” and the curved bubble surface due to jet impact;<sup>22</sup> a similar scenario is described in Ohi and Iking.<sup>49</sup> But there are no results of exactly the same experimental basic conditions, which can be found in the publications about the interaction of two spatially separated cavitation bubbles.

A special case of interaction behavior can be distinguished for the highest analyzed energy ratio of (4.0:2.0) times the breakdown threshold. At large bubble distances, weak bubble-bubble interaction leads to a scarcely identifiable influence on the oscillation dynamics of both bubbles; however, there is no observable second oscillation cycle of the smaller bubble except for the largest bubble distance. Apart from asymmetric water flows that accompany the collapse phase, no directed water jet penetrating the higher energetic bubble can be detected at any bubble distance. Pearson *et al.* report considerable dependence of the jet impact on the distance between a cavitation bubble and a rigid boundary,<sup>43</sup> similar to the phenomena described here. The higher energetic bubble seems to suppress the formation of the other. The situation becomes apparent in a slight decrease of the maximum bubble radius  $r_{\max}$  for a comparably small bubble distance as well as in an almost complete rejection of the oscillation cycle of the smaller cavitation bubble for bubble distances, which correspond to a bubble overlap. The observed distance where a contact between both bubbles is observable is contrary to the value expected from geometrical considerations (cf. Section 3.2); this also supports the thesis of suppression proposed before.

## 5 Conclusion

We presented the dynamic interaction of two cavitation bubbles generated close to each other by focused ultrashort laser pulses using time-resolved photography. The interaction between equally sized (generated at the same laser pulse energy) cavitation bubbles generated simultaneously, as studied in

Section 3.1, is very instructive in the study and quantification of the different constitutional interaction modes. Yet, this scenario does not accurately reflect the situation found in laser surgery, because both bubbles are at the same stage of temporal evolution at each time. To our best knowledge, there is no series of systematic investigations in which the behavior of cavitation bubble interaction was studied regarding the dissection quality during therapeutic applications of fs-lasers in ophthalmology. The analogy to a single oscillating cavitation bubble near a rigid boundary enabled us to discuss our results in the context of basic principles established in the field of fluid mechanics.

The interaction between two cavitation bubbles generated at different energies, as studied in Section 3.2, resembles the situation found in a modern laser surgery where pulses are applied consecutively at high repetition rate; because the bubbles are at different oscillation stages, they display a phase difference.

For the sake of simplicity, water has been used here as a model medium. It is not clear how effects such as liquid jet formation or a flowing of the medium play out in biological tissues.<sup>40</sup> However, the observations made in water clearly suggest the generation of strong mechanical forces, which would affect the surrounding tissue. If we infer from the case of an energy ratio between two bubbles, about to the case of pulses being applied consecutively in time, then the jet directed toward the other bubble would always point in the direction of laser scanning, leading to modification of tissue not yet irradiated. Possibly, this could produce further tissue dissection in the direction of the feed motion due to the previously applied laser pulses, thus enhancing the efficiency of tissue cutting.

In summary, our study is the first to use a restricted range of laser parameters to study cavitation bubble dynamics (e.g., pulse energy and repetition rate), which present a more realistic model of the current development of ultrashort pulse lasers for clinical applications. Experimental scanning procedures for spatial and temporal pulse separation will further allow further analysis of the interaction of multiple cavitation bubbles. Their influence on the overall dissection quality of tissue will be determined by extending the study to biological samples.

## Acknowledgment

Nadine Tinne acknowledges support from the fellowship “Foundation of German Business,” Berlin, Germany (funded by Germany’s Federal Ministry for Education and Research). Dr. Valeria Nuzzo acknowledges support from the fellowship “jeune post-doc,” École Polytechnique, Paris, France.

## References

1. P. S. Binder, “One thousand consecutive IntraLase laser *in situ* keratomileusis flaps,” *J. Cataract Refract. Surg.* **32**(6), 962–969 (2006).
2. T. Juhasz, F. Loesel, C. Horvath, R. Kurtz, J. Bille, and G. Mourou, “Corneal refractive surgery with femtosecond lasers,” *IEEE J. Quantum Electron.* **5**(4), 902–910 (1999).
3. G. M. Kerzorian and K. G. Stonecipher, “Comparison of the IntraLase femtosecond laser and mechanical keratomes for laser *in situ* keratomileusis,” *J. Cataract Refract. Surg.* **30**(4), 804–811 (2004).
4. H. Lubatschowski, G. Maatz, A. Heisterkamp, U. Hetzel, W. Drommer, H. Welling, and W. Ertmer, “Application of ultrashort laser pulses for intrastromal refractive surgery,” *Graef. Arch. Clin. Exp.* **238**(1), 33–39 (2000).

5. I. Ratkau-Traub, I. E. Ferincz, T. Juhasz, R. M. Kurtz, and R. R. Krueger, "First clinical results with the femtosecond neodymium-glass laser in refractive surgery," *J. Refract. Surg.* **19**(2), 94–103 (2003).
6. T. Ripken, "Anwendung von MHz-fs-Lasern in der Ophthalmologie und Erarbeitung eines Therapiekonzeptes für die laserassistierte Behandlung der Alterssichtigkeit," *Ph.D. Thesis, University Hanover, Germany* (2007).
7. T. Ripken, U. Oberheide, M. Fromm, S. Schumacher, G. Gerten, and H. Lubatschowski, "Fs-laser induced elasticity changes to improve presbyopic lens accommodation," *Graef. Arch. Clin. Exp.* **246**(6), 897–906 (2008).
8. Z. Nagy, A. Takacs, T. Filkorn, and M. Sarayba, "Initial clinical evaluation of an intraocular femtosecond laser in cataract surgery," *J. Refract. Surg.* **25**, 1053–1060 (2009).
9. M. C. Knorz and U. Vossmerbaeumer, "Comparison of flap adhesion strength using the amadeus Microkeratome and the IntraLase iFS femtosecond laser in rabbits," *J. Refract. Surg.* **24**(9), 875–878 (2008).
10. H. Lubatschowski, "Overview of commercially available femtosecond lasers in refractive surgery," *J. Refract. Surg.* **24**, 102–107 (2008).
11. C. L. Arnold, A. Heisterkamp, W. Ertmer, and H. Lubatschowski, "Computational model for nonlinear plasma formation in high NA micromachining of transparent materials and biological cells," *Opt. Express* **15**(16), 10303–10317 (2007).
12. P. K. Kennedy, D. X. Hammer, and B. A. Rockwell, "Laser-induced breakdown in aqueous media," *Prog. Quantum Electron.* **21**(3), 155–248 (1997).
13. J. Noack and A. Vogel, "Laser-induced plasma formation in water at nanosecond to femtosecond time scales: calculation of thresholds, absorption coefficients, and energy density," *IEEE J. Quantum Electron.* **35**(8), 1156–1167 (1999).
14. C. A. Sacchi, "Laser-induced electric breakdown in water," *J. Opt. Soc. Am. B* **8**(2), 337–345 (1991).
15. H. Lubatschowski and A. Heisterkamp, "Interaction with biological tissue" in *Femtosecond Technology for Technical and Medical Applications*, F. Dausinger, F. Lichtner, and H. Lubatschowski, Eds., Springer-Verlag, Heidelberg (2004).
16. V. Nuzzo, K. Plamann, M. Savoldelli, M. Merano, D. Donate, O. Albert, P. F. Gardeazabal Rodríguez, G. Mourou, and J. M. Legeais, "In situ monitoring of second harmonic generation in human corneas to compensate for femtosecond laser pulse attenuation in keratoplasty," *J. Biomed. Opt.* **12**(6), 064032 (2007).
17. A. Vogel, K. Nahen, D. Theisen, R. Birngruber, R. J. Thomas, and B. A. Rockwell, "Influence of optical aberrations on laser-induced plasma formation in water and their consequences for intraocular photodisruption," *Appl. Opt.* **38**(16), 3636–3643 (1999).
18. A. Vogel, N. Linz, S. Freidank, and G. Paltauf, "Femtosecond-laser-induced nanocavitation in water: implications for optical breakdown threshold and cell surgery," *Phys. Rev. Lett.* **100**(3), 038102 (2008).
19. J. Noack, D. X. Hammer, G. D. Noojin, B. A. Rockwell, and A. Vogel, "Influence of pulse duration on mechanical effects after laser-induced breakdown in water," *J. Appl. Phys.* **83**(12), 7488–7495 (1998).
20. W. Lauterborn, "Kavitation durch Laserlicht," *Acustica* **31**(2), 51–78 (1974).
21. W. Lauterborn and W. Hentschel, "Cavitation bubble dynamics studied by high speed photography and holography: Part 1," *Ultrasonics* **23**(3), 260–268 (1985).
22. W. Lauterborn and C.-D. Ohl, "The peculiar dynamics of cavitation bubbles," *Appl. Sci. Res.* **58**, 63–76 (1998).
23. P. A. Quinto-Su and C.-D. Ohl, "Interaction between two laser-induced cavitation bubbles in a quasi-two dimensional geometry," *J. Fluid Mech.* **633**, 425–435 (2009).
24. A. Shima, "Studies on bubble dynamics," *Shock Waves* **7**, 33–42 (1997).
25. Y. Tomita, A. Shima and K. Sato, "Dynamic behavior of two-laser-induced bubbles in water," *Appl. Phys. Lett.* **57**(3), 234–236 (1990).
26. Y. Tomita and A. Shima, "High-speed photographic observations of laser-induced cavitation bubbles in water," *Acustica* **71**, 161–171 (1990).
27. S. Rungsiyaphornrat, E. Klaseboer, B. C. Khoo, and K. S. Yeo, "The merging of two gaseous bubbles with an application to underwater explosions," *Comput. Fluids* **32**(8), 1049–1074 (2003).
28. S. Schumacher, "Entwicklung einer Ultrakurzpuls-Laserapplikationseinheit zur Behandlung der Alterssichtigkeit," *Ph.D. Thesis, Gottfried Wilhelm Leibniz University Hanover, Germany* (2009).
29. O. Kermani and U. Oberheide, "Comparative micromorphologic in vitro porcine study of IntraLase and Femto LDV femtosecond lasers," *J. Cataract Refract. Surg.* **34**, 1393–1399 (2008).
30. A. Vogel, J. Noack, K. Nahen, D. Theisen, S. Busch, U. Parltitz, D. X. Hammer, G. D. Noojin, B. A. Rockwell, and R. Birngruber, "Energy balance of optical breakdown at nanosecond to femtosecond time scales," *Proc. SPIE* **3255**, 34–43 (1998).
31. A. Vogel, "Optical breakdown in water and ocular media, and its use for intraocular photodisruption," *Habilitation Dissertation, Medical University of Lübeck, Germany* (1998).
32. K. Jungnickel and A. Vogel, "Interaction of two laser-induced cavitation bubbles" in *Bubble Dynamics and Interface Phenomena*, J. R. Blake, J. M. Boulton-Stone and N. H. Thomas, Eds., Kluwer Academic Publishers, Dordrecht (1994).
33. P. Testud-Giovanneschi, A. P. Alioncle, and D. Dufresne, "Collective effects of cavitation: Experimental study of bubble-bubble and bubble-shock wave interactions," *J. Appl. Phys.* **67**(8), 3560–3564 (1989).
34. J. R. Blake, P. B. Robinson, A. Shima, and Y. Tomita, "Interaction of two cavitation bubbles with a rigid boundary," *J. Fluid Mech.* **255**, 707–721 (1993).
35. C.-D. Ohl and E. Ory, "Aspherical bubble collapse—comparison with simulations," in *Proc. AIP Conf. ISNA*, Vol. **15**, pp. 393–396 (2000).
36. J. R. Blake and D. C. Gibson, "Cavitation bubbles near boundaries," *Annu. Rev. Fluid Mech.* **19**, 99–123 (1987).
37. J. R. Blake, G. S. Keen, R. P. Tong, and M. Wilson, "Acoustic cavitation: the fluid dynamics of non-spherical bubbles," *Philos. Trans. R. Soc. A* **357**, 251–267 (1999).
38. E. A. Brujan, G. S. Keen, A. Vogel, and J. R. Blake, "The final stage of the collapse of a cavitation bubble close to a rigid boundary," *Phys. Fluids* **14**(1), 85–92 (2002).
39. E. Klaseboer, K. C. Hung, C. Wang, C. W. Wang, B. C. Khoo, P. Boyce, S. Debono, and H. Charlier, "Experimental and numerical investigation of the dynamics of an underwater explosion bubble near a resilient/rigid structure," *J. Fluid Mech.* **537**, 387–413 (2005).
40. T. Kodama and Y. Tomita, "Cavitation bubble behavior and bubble-shock wave interaction near a gelatine surface as a study of in vivo bubble dynamics," *Appl. Phys. B* **70**, 139–149 (2000).
41. Y. Tomita and A. Shima, "Mechanisms of impulsive pressure generation and damage pit formation by bubble collapse," *J. Fluid Mech.* **169**, 535–564 (1986).
42. Y. Tomita and T. Kodama, "Interaction of laser-induced cavitation bubbles with composite surfaces," *J. Appl. Phys.* **94**(5), 2809–2816 (2003).
43. A. Pearson, J. R. Blake, and S. R. Otto, "Jets in bubbles," *J. Eng. Math.* **48**, 391–412 (2004).
44. I. Akhatov, O. Lindau, A. Topolnikov, R. Mettin, N. Vakhitova, and W. Lauterborn, "Collapse and rebound of a laser-induced cavitation bubble," *Phys. of Fluids* **13**(10), 2805–2819 (2001).
45. R. Geisler, "Untersuchungen zur laserinduzierten Kavitation mit Nanosekunden- und Femtosekundenlasern," *Ph.D. Thesis, Georg August University Göttingen, Germany* (2003).
46. Y. Tomita, M. Tsubota, K. Nagane, and N. An-naka, "Behavior of laser-induced cavitation bubbles in liquid nitrogen," *J. Appl. Phys.* **88**(10), 5993–6001 (2000).
47. A. Heisterkamp, "Einsatz ultrakurzer Laserpulse in der refraktiven Laserchirurgie," *Ph.D. Thesis, University Hanover, Germany* (2002).
48. C. Wang and B. C. Khoo, "An indirect boundary element method for three-dimensional explosion bubbles," *J. Comput. Phys.* **194**, 451–480 (2004).
49. C.-D. Ohl and R. Iking, "Shock-wave-induced jetting of micron-size bubbles," *Phys. Rev. Lett.* **90**(21), 214502 (2003).